




Article

Synthesis, X-ray Structure and Biological Studies of New Self-Assembled Cu(II) Complexes Derived from *s*-Triazine Schiff Base Ligand

Tarek E. Khalil ^{1,*} , Kholood A. Dahlous ^{2,*}, Saied M. Soliman ^{1,*} , Nessma A. Khalil ¹, Ayman El-Faham ¹  and Ali El-Dissouky ¹

- ¹ Department of Chemistry, Faculty of Science, Alexandria University, P.O. Box 426, Ibrahimia, Alexandria 21321, Egypt; nessma_1988@outlook.com (N.A.K.); aymanel_faham@hotmail.com (A.E.-F.); alioldissouky@alexu.edu.eg (A.E.-D.)
- ² Department of Chemistry, College of Science, King Saud University, P.O. Box 2455, Riyadh 11451, Saudi Arabia
- * Correspondence: tarekake@alexu.edu.eg (T.E.K.); kdahlous@ksu.edu.sa (K.A.D.); saied1soliman@yahoo.com (S.M.S.)

Abstract: The two ligands 2-(1-(2-(4,6-dimorpholino-1,3,5-triazin-2-yl)hydrazono)ethyl)aniline (**DMAT**) and 2-(1-(2-(4,6-dimorpholino-1,3,5-triazin-2-yl)hydrazono)ethyl)phenol (**DMOHT**) were used to synthesize three heteroleptic Cu(II) complexes via a self-assembly technique. The structure of the newly synthesized complexes was characterized using elemental analysis, FTIR and X-ray photoelectron spectroscopy (XPS) to be [Cu(DMAT)(H₂O)(NO₃)]NO₃·C₂H₅OH (**1**), [Cu(DMOT)(CH₃COO)] (**2**) and [Cu(DMOT)(NO₃)] (**3**). X-ray single-crystal structure of complex **1** revealed a hexa-coordinated Cu(II) ion with one **DMAT** as a neutral tridentate *NNN*-chelate, one bidentate nitrate group and one water molecule. In the case of complex **2**, the Cu(II) is tetra-coordinated with one **DMOT** as an anionic tridentate *NNO*-chelate and one monodentate acetate group. The antimicrobial, antioxidant and anticancer activities of the studied compounds were examined. Complex **1** had the best anticancer activity against the lung carcinoma A-549 cell line (IC₅₀ = 5.94 ± 0.58 μM) when compared to *cis*-platin (25.01 ± 2.29 μM). The selectivity index (SI) of complex **1** was the highest (6.34) when compared with the free ligands (1.3–1.8), and complexes **2** (0.72) and **3** (2.97). The results suggested that, among those compounds studied, complex **1** is the most promising anticancer agent against the lung carcinoma A-549 cell line. In addition, complex **1** had the highest antioxidant activity (IC₅₀ = 13.34 ± 0.58 μg/mL) which was found to be comparable to the standard ascorbic acid (IC₅₀ = 10.62 ± 0.84 μg/mL). Additionally, complex **2** showed broad-spectrum antimicrobial action against the microbes studied. The results revealed it to possess the strongest action of all the three complexes against *B. subtilis*. The MIC values found are 39.06, 39.06 and 78.125 μg/mL for complexes **1–3**, respectively.

Keywords: *s*-Triazine; Cu(II) complexes; antimicrobial; antioxidant; anticancer; lung carcinoma



Citation: Khalil, T.E.; Dahlous, K.A.; Soliman, S.M.; Khalil, N.A.; El-Faham, A.; El-Dissouky, A. Synthesis, X-ray Structure and Biological Studies of New Self-Assembled Cu(II) Complexes Derived from *s*-Triazine Schiff Base Ligand. *Molecules* **2022**, *27*, 2989. <https://doi.org/10.3390/molecules27092989>

Academic Editor: Maria Paula Marques

Received: 11 April 2022

Accepted: 3 May 2022

Published: 6 May 2022

Publisher's Note: MDPI stays neutral with regard to jurisdictional claims in published maps and institutional affiliations.



Copyright: © 2022 by the authors. Licensee MDPI, Basel, Switzerland. This article is an open access article distributed under the terms and conditions of the Creative Commons Attribution (CC BY) license (<https://creativecommons.org/licenses/by/4.0/>).

1. Introduction

Hydrazones have been considered as initiating compounds for most of synthetic chemistry, offering multifunctional benefits to various fields, such as industrial and pharmacological applications [1–7]. They have played an essential role in analytical and medicinal chemistry, as well as in coordination chemistry as polydentate ligands because of their versatile chelating capacity with most transition metals [8–12]. On the other hand, Schiff base hydrazone derivatives have attracted great attention because of their valuable applications as heterogeneous catalysts, molecular switching materials and analytical reagents, and for their use in forming covalent organic frameworks [13–15]. Additionally, they have been demonstrated to be bioactive compounds that can be widely used for the treatment of

many diseases caused by some types of bacteria and viruses; they inhibit the replication of these viruses or bacteria inside living cells. Hydrazones have shown encouraging results as antidepressants, antimalarial, anticancer, anti-inflammatory, and antioxidant agents as well [16–20].

On the other hand, *s*-Triazines play integral roles as a organic ligands in coordination chemistry [21–27] and as organic building units in supramolecular chemistry [28–30]. Another advantage is the synthetic versatility of *s*-Triazine derivatives which comes from the simple and inexpensive way they can be prepared from cyanuric chloride [31–33]. *s*-Triazines exhibit a wide range of industrial and agricultural uses, including in the preparation of resins, dyes for textiles, removal agents for sulfide and in herbicides [34,35]. In addition, they have an essential position in medicinal chemistry since they are used in the manufacturing of many drugs with various pharmacological activities [36,37]. Additionally, Schiff bases containing *s*-Triazine have a wide range of biological activities, especially as promising anticancer agents [38–41]. Over and above these, Cu(II) complexes with *s*-Triazine hydrazone derivatives have interesting magnetic and catalytic applications [42–46], as they play a catalytic role in numerous chemical and biological processes, concurrently performing an essential function in the immune system, nutrient metabolism, as well as serving as a metal cofactor bound to protein in the living body. Although copper is a trace metal, its numerous complexes are now gaining attention because of their prospective uses as antiviral, antibacterial, anti-inflammatory drugs with decreased unwanted effects and as anticancer medicines [47–54].

Motivated by the facts outlined above, the current study focuses on the synthesis and spectroscopic characterizations of three new Cu(II) complexes with the 2-(hydrazino)-4,6-disubstituted-*s*-Triazine ligands shown in Figure 1. X-ray diffraction of single-crystal, Hirshfeld, and spectroscopic analyses were used to investigate the structural characteristics of the synthesized complexes. Furthermore, the antibacterial, antioxidant and anticancer activities of these complexes were studied and compared with free ligands.

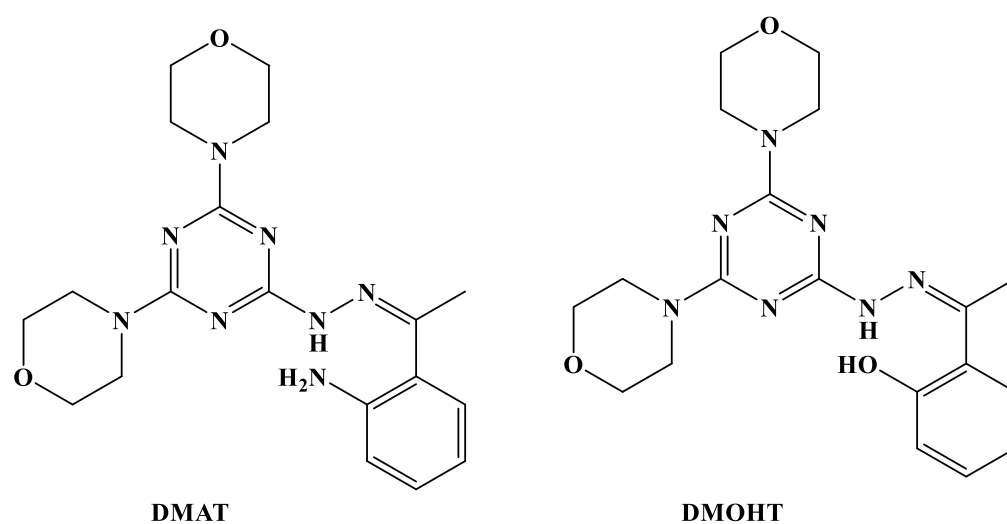


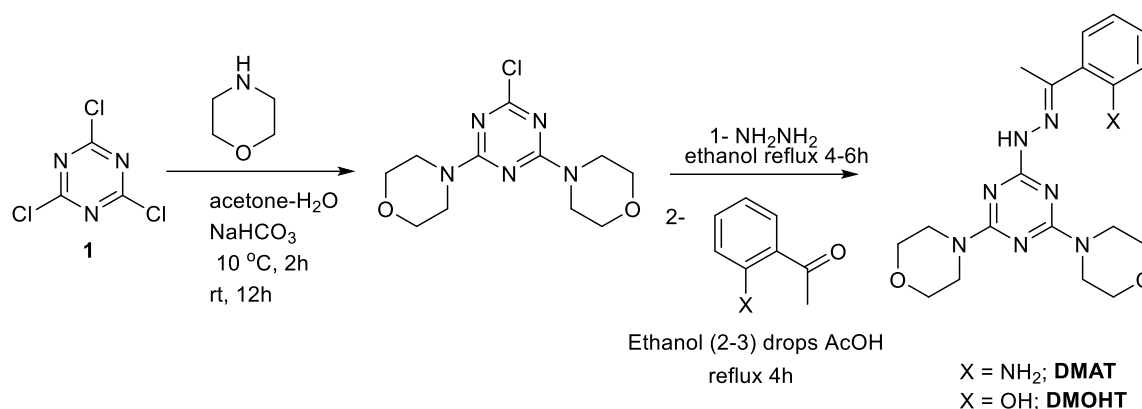
Figure 1. Structures of the studied ligands.

2. Results and Discussion

2.1. Synthesis and Characterizations

The two ligands **DMAT** and **DMOHT** were prepared following the reported method [55]. The first and second chlorine atoms of the 2,4,6-trichloro-1,3,5-triazine (cyanuric chloride) were replaced in one step by two morpholine. Then the third chlorine atom was replaced by hydrazine under reflux for 4–6 h (Scheme 1). Finally, the hydrazine derivatives were condensed with 2-amino-/or 2-hydroxy-acetophenone in the presence of a few drops of acetic acid and ethanol as a solvent in order to give the target products in high yields and

with high purities, as observed from their NMR spectra, which are in good agreement with the reported data (Figures S1 and S2; Supplementary material).



Scheme 1. Synthesis of DMAT and DMOHT.

The three new Cu(II) complexes were synthesized using a self-assembly technique. The newly synthesized complexes were characterized using FTIR, elemental analysis and X-ray photoelectron spectroscopy (XPS). The FTIR spectra of the studied complexes are shown in Figures S3 and S4 (Supplementary material). The schematic presentation for the proposed structures of the studied complexes is presented in Figure 2. The structures of two of the newly synthesized complexes were further confirmed using single-crystal X-ray diffraction. The results were found to be in accordance with the proposed structures based on the analytical and spectral analyses.

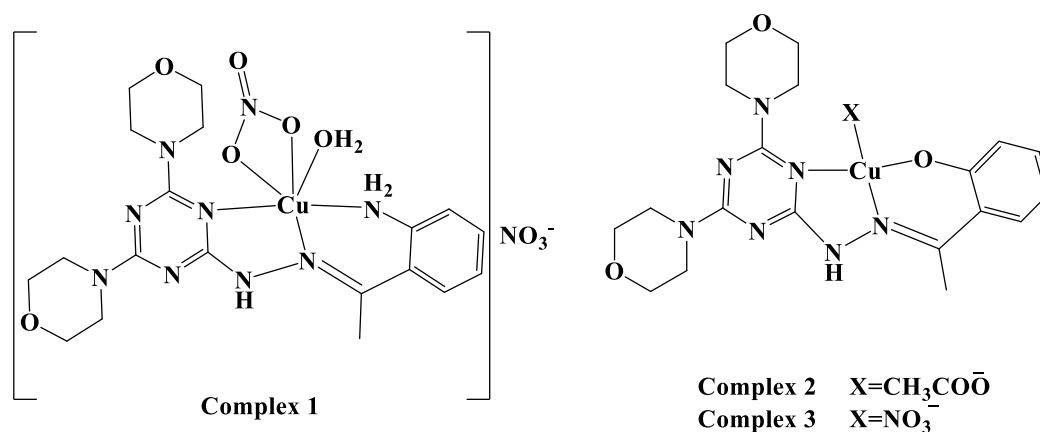


Figure 2. Structures of the synthesized Cu(II) complexes.

2.2. X-ray Structure

2.2.1. Structure Description of Complex 1

The X-ray structure together with the atomic numbering of the $[\text{Cu}(\text{DMAT})(\text{H}_2\text{O})(\text{NO}_3)]\text{NO}_3 \cdot \text{C}_2\text{H}_5\text{OH}$ complex (**1**) are shown in Figure 3. A list of the most important geometric parameters is given in Table 1. Complex **1** crystallized in the triclinic crystal system and P-1 space group and $Z = 2$ (Table S1; Supplementary material). The Cu(II) was coordinated with one neutral **DMAT** ligand as a tridentate *NNN*-chelate, with one water molecule and a nitrate group leading to the cationic coordination sphere $[\text{Cu}(\text{DMAT})(\text{H}_2\text{O})(\text{NO}_3)]^+$. The outer sphere comprised one nitrate counter anion and one highly disordered ethanol molecule. The coordination centers of the organic ligand were the N-sites from the amino group, hydrazone and triazine moieties. All of the three Cu-N distances recorded are marginally different (Table 1). The N1-Cu1-N2 (88.17(9)) and the N2-Cu1-N4 (82.26(8)) bite angles of the **DMAT** ligand led to the stable six membered and five membered chelate

rings, respectively. The coordination environment of the Cu(II) was completed by two strong interactions with one oxygen atom from the coordinated nitrate (Cu1-O4; 2.006(2) Å) and another oxygen atom from a water molecule (Cu1-O1; 2.185(2) Å) augmented with an extra weak interaction with an oxygen atom from the same nitrate group (Cu1-O5; 2.651(2) Å). Hence, the coordination number of Cu(II) found was six, and the nitrate group acting as a bidentate ligand where the bite angle of the bidentate nitrate group was only 53.28(8)°.

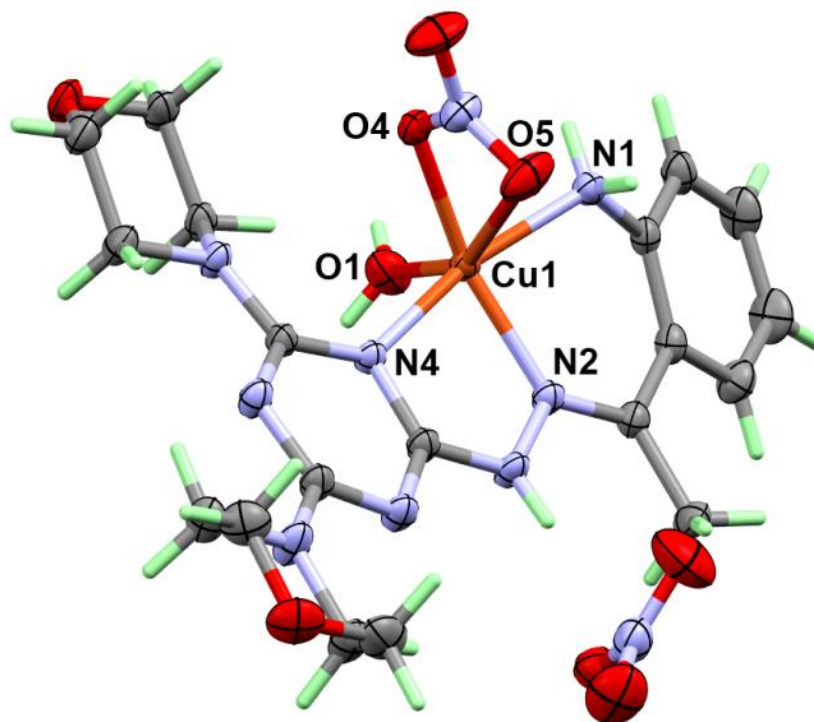


Figure 3. Structure and atomic numbering of complex 1. The disordered ethanol molecule was omitted for better clarity.

Table 1. The most important bond distances (Å) and angles (°) of complex 1.

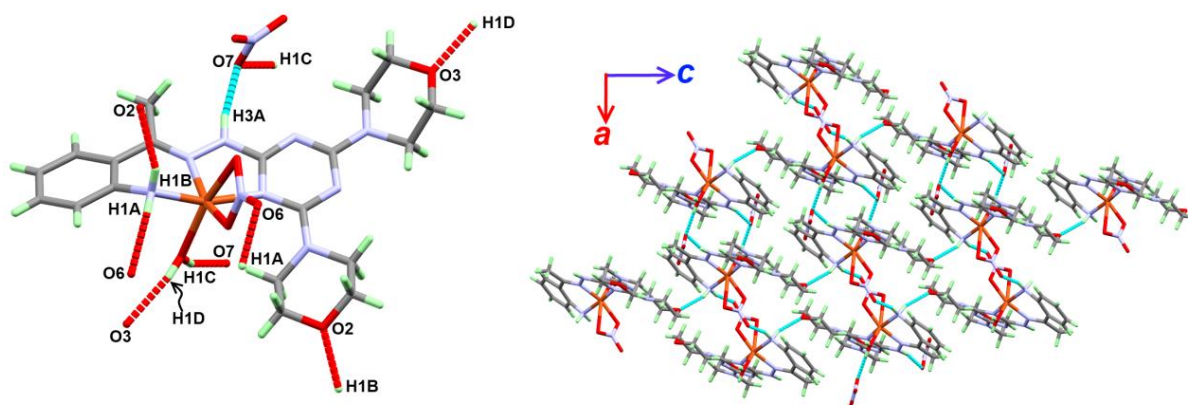
Bond	Distance	Bond	Distance
Cu1-N1	1.989 (2)	Cu1-O4	2.006 (2)
Cu1-N2	1.990 (2)	Cu1-O1	2.185 (2)
Cu1-N4	2.022 (2)	Cu1-O5	2.651 (2)
Bonds	Angle	Bonds	Angle
N1-Cu1-N4	163.73 (9)	O4-Cu1-N4	95.83 (8)
N1-Cu1-O1	92.13 (9)	O4-Cu1-O1	103.61 (9)
N1-Cu1-O4	88.16 (9)	O5-Cu1-O4	53.28 (8)
N2-Cu1-N4	82.26 (8)	O5-Cu1-N1	83.17 (9)
N2-Cu1-O1	98.06 (10)	O5-Cu1-N2	104.87 (9)
N2-Cu1-O4	158.14 (9)	O5-Cu1-N4	86.58 (9)
N4-Cu1-O1	102.19 (9)	O5-Cu1-O1	156.38 (9)
N1-Cu1-N2	88.17 (9)		

The molecular packing of complex 1 was controlled by strong N-H...O and O-H...O hydrogen bonding interactions (Table 2). The presentation of these contacts is shown in the left part of Figure 4, while the right part of the same figure presents the packing along the *ac* plane. The N-H of the amino groups and the O-H of the water molecule are the hydrogen bond donors, while the hydrogen bond acceptor sites are the oxygen atoms that are either from the nitrate or morpholine moieties.

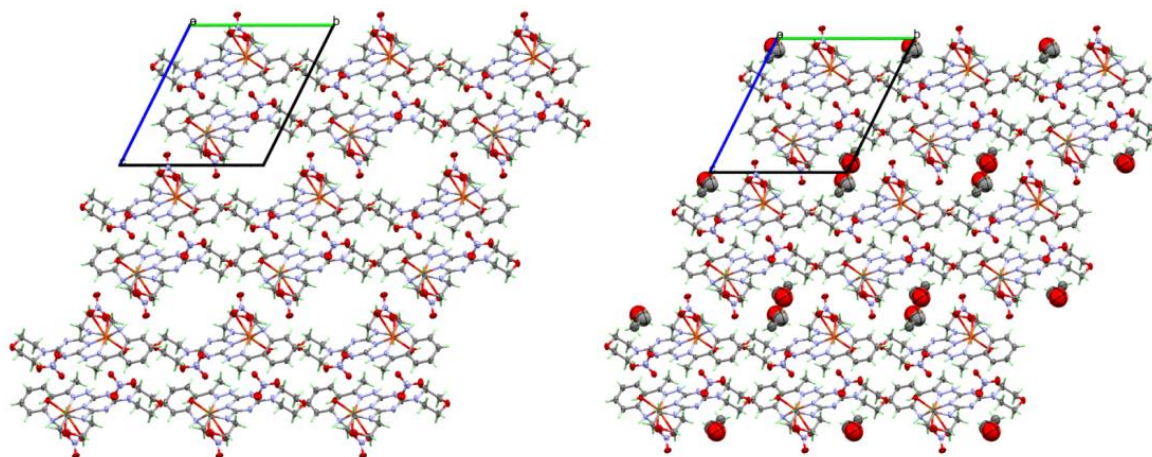
Table 2. The hydrogen bond parameters of complexes 1 and 2.

Atoms	D-H (Å)	H...A (Å)	D...A (Å)	D-H...A (°)
N1-H1A...O6 ⁱ	0.84 (3)	2.17 (4)	2.975 (4)	161 (3)
N1-H1B...O2 ⁱⁱ	0.85 (3)	2.14 (3)	2.932 (3)	155 (2)
O1-H1C...O7 ⁱⁱⁱ	0.81 (3)	2.01 (3)	2.787 (4)	162 (4)
O1-H1D...O3 ^{iv}	0.79 (4)	2.00 (4)	2.767 (4)	163 (4)
N3-H3A...O7	0.84 (3)	2.12 (3)	2.936 (4)	165 (3)

Symm. Code: (i) 2-x,1-y,1-z; (ii) -1 + x,y,z; (iii) 2-x,1-y,1-z; (iv) x,1 + y,z

**Figure 4.** The hydrogen bond contacts (left) and packing along the *ac* plane (right).

It is worth noting that the crystallized ethanol molecules occupy the spaces among the complex units and are located in between the coordinated and ionic nitrate anions along the *b* and *c* directions, which further aid in the supramolecular structure of the studied complex. For a better understanding, the packing structures of the complex units with and without the solvent molecule are depicted in Figure 5. Unfortunately, the corresponding hydrogen bond parameters could not be correctly determined because of the presence of strong disorder in the ethanol molecule.

**Figure 5.** The packing structures of complex 1 with (left) and without (right) the disordered ethanol molecule.

2.2.2. Structure Description of Complex 2

The X-ray structure of complex 2 satisfactorily revealed the tetra-coordination environment of the Cu(II). This complex crystallized in the more symmetric monoclinic crystal system and the $P2_1/n$ space group while the unit cell comprised four molecules ($Z = 4$) (Table S1; Supplementary material). The structure of the coordination sphere of complex 2

could be simply described as $[\text{Cu}(\text{DMOT})(\text{CH}_3\text{COO})]$. In this neutral complex, the organic ligand acted as a mononegative tridentate *NNO*-chelate, where the hydroxyl group was deprotonated during the course of the preparation owing to the presence of the relatively strong basic acetate anion (Figure 6).

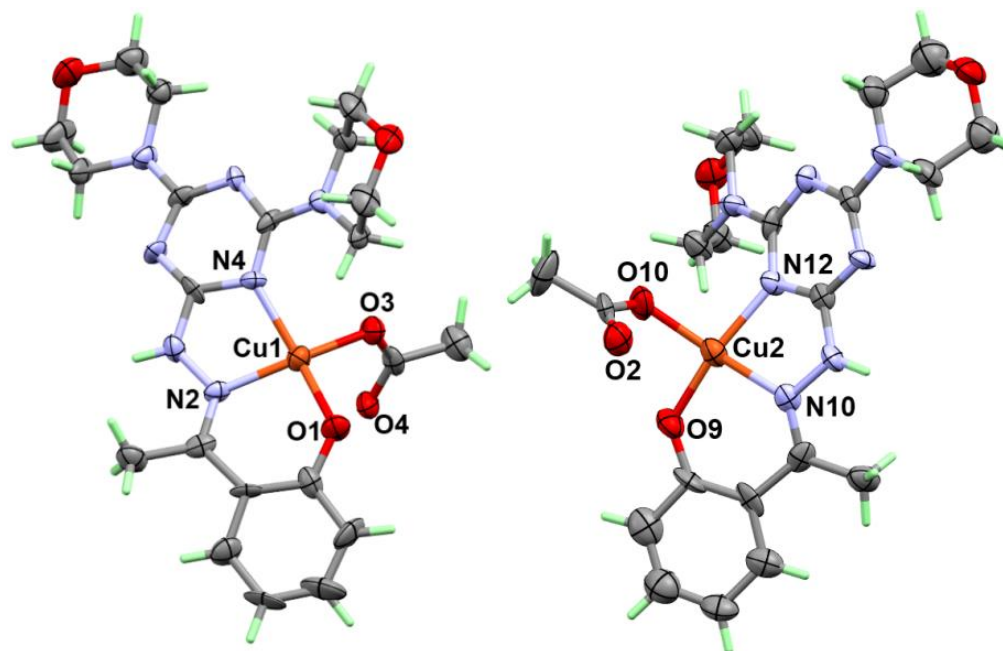


Figure 6. Structure and atom numbering of the coordination sphere of complex 2.

There are two molecular units that can be described as an asymmetric formula, where the two Cu(II) centers have similar coordination spheres and differ very little in Cu-N and Cu-O distances (Table 3). It is clear from the table below that the Cu-N_(hydrazone) bonds are slightly shorter than the Cu-N_(s-Triazine) in both complexes. Generally, the Cu-N distances are shorter in complex 2 when compared to those found in complex 1. The tetra-coordination environment of the Cu(II) is completed by one coordinated acetate ion as a monodentate ligand. The Cu-O distances are found to be 1.905(7) Å (Cu1-O3) and 1.902(8) Å (Cu2-O10), which are generally longer than the distances between the Cu(II) and the phenolic oxygen atom. The distances between the Cu1 and Cu2 centers to the O4 and O2 atoms of the acetate anion were found to be 2.961(6) and 2.953(7) Å, respectively, both of which are too long to be bonds. Hence, the acetate anion in both units could be described as a monodentate ligand. The coordination geometry around Cu(II) could be described as a distorted square planar; the packing scheme is shown in Figure 7.

Table 3. The most important bond distances (Å) and angles (°) for complex 2.

Bond	Distance	Bond	Distance
Cu1-O3	1.905(7)	Cu2-O10	1.902(8)
Cu1-O1	1.873(6)	Cu2-O9	1.852(7)
Cu1-N2	1.945(8)	Cu2-N10	1.938(8)
Cu1-N4	1.976(7)	Cu2-N12	1.984(8)
Bonds	Angle	Bonds	Angle
O3-Cu1-N2	160.9(3)	O10-Cu2-N10	164.1(3)
O3-Cu1-N4	97.4(3)	O10-Cu2-N12	96.2(3)
O1-Cu1-O3	93.0(3)	O9-Cu2-O10	92.5(3)
O1-Cu1-N2	93.2(3)	O9-Cu2-N10	92.5(4)
O1-Cu1-N4	160.2(3)	O9-Cu2-N12	163.9(3)
N2-Cu1-N4	82.4(3)	N10-Cu2-N12	82.1(4)

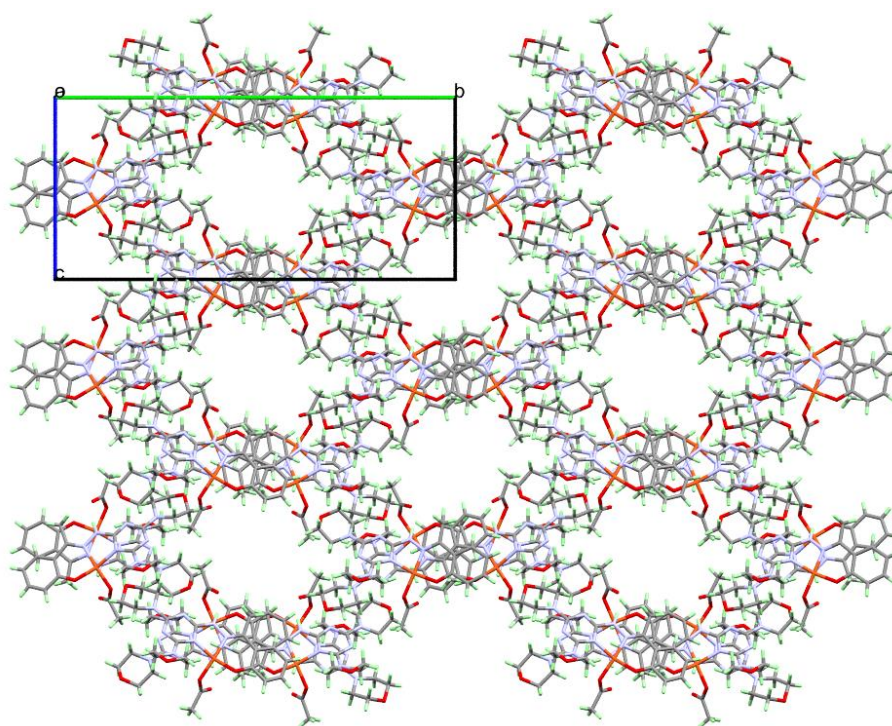


Figure 7. Packing scheme of the complex units of **2**. In such tubular structures, these spaces are occupied by the highly disordered solvent (water) molecules, where their protons could not be refined properly.

2.3. Analysis of Molecular Packing

Hirshfeld maps are characteristic of each crystal, and our analysis of these maps gave us quite a clear idea about the intermolecular interactions included in the molecular packing within a crystal. The distribution of the different contacts for complexes **1** and **2** are presented in Figure 8. In the case of complex **1**, the percentages of the O...H, H...H and H...C contacts are the highest. Their percentages are 37.2, 43.0 and 11.8%, respectively. Analysis of the fingerprint plot of complex **1** revealed that both O...H and H...H are short contacts, as these interactions appeared as sharp spikes (Figure 9). The regions included in the H...H and O...H interactions are labelled in the d_{norm} map as regions **A** and **B**, respectively (Figure 10). These regions are marked with a red color, further indicating interactions shorter than the vdWs radii sum of the interacting atoms.

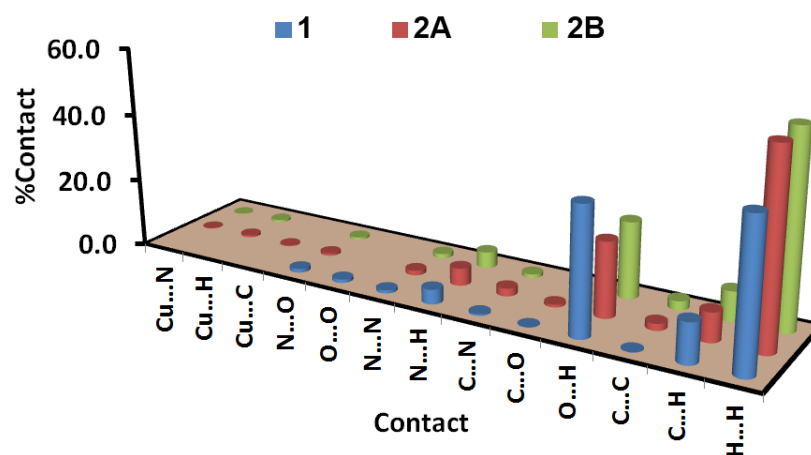


Figure 8. The intermolecular interactions in complexes **1** and **2**.

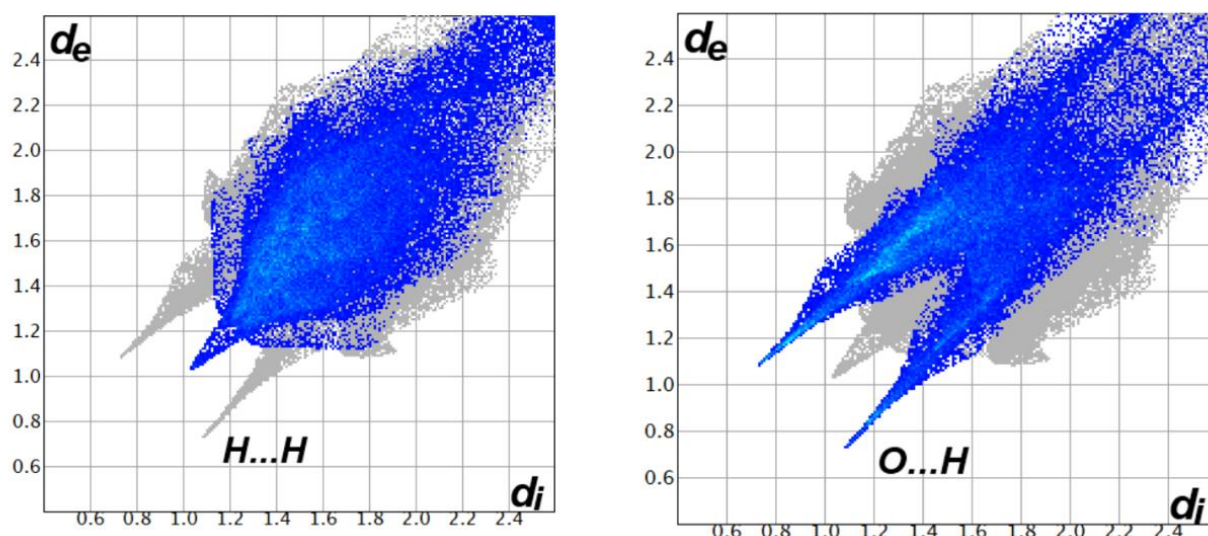


Figure 9. Decomposed fingerprint plots in complex 1.

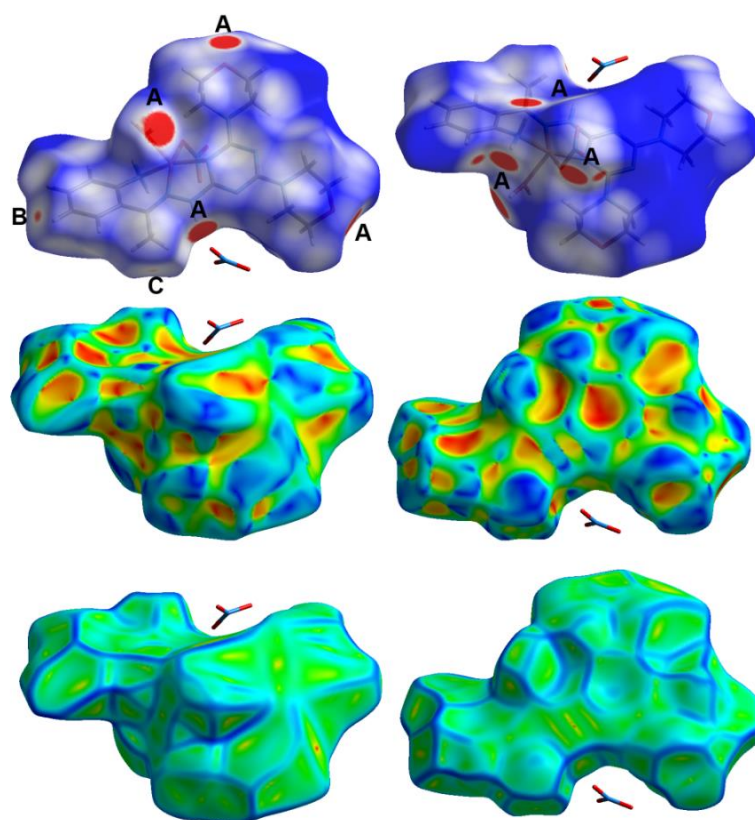


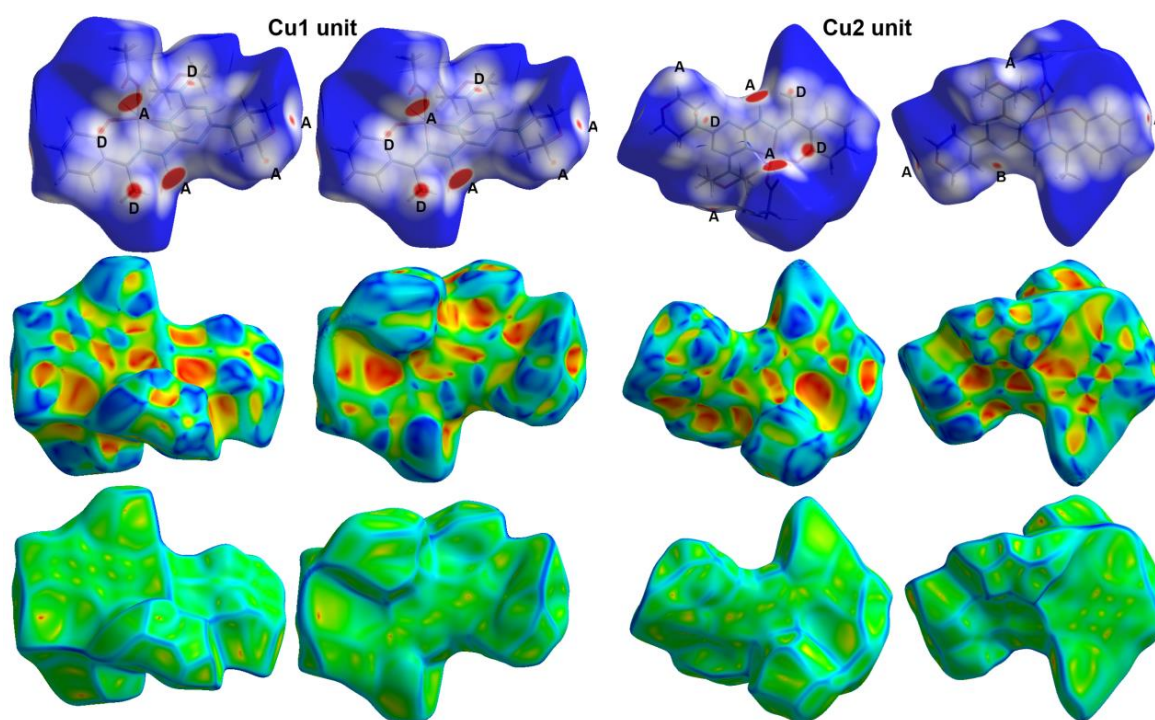
Figure 10. Hirshfeld maps of complex 1. The most important interactions are (A) O ... H, (B) H ... H and (C) C ... C.

The shortest O ... H interactions are O7 ... H1C and O3 ... H1D, where the hydrogen-acceptor distances are 1.841 and 1.820 Å, respectively. Generally, there are quite a large number of O ... H interactions, with hydrogen-acceptor distances ranging from 1.820 Å to 2.601 Å (O5 ... H14A). Additionally, there are two other short interactions which belong to H4 ... H4 (2.074 Å) and C11 ... C11 (3.350 Å)—interactions which are considered important in the molecular packing of 1. A summary of short contacts is listed in Table 4.

Table 4. The short-distance interactions and their distances.

Contact	Distance	Contact	Distance
1		2	
O5 ... H14A	2.601	O8 ... H3A	2.397
O2 ... H1B	1.996	O4 ... H11	1.857
O7 ... H1C	1.841	O2 ... H3	1.802
O8 ... H1C	2.543	O5 ... H24	2.483
O3 ... H1D	1.820	O7 ... H40A	2.584
O8 ... H19A	2.577	O6 ... H16B	2.551
O6 ... H2A	2.419	O6 ... H35B	2.361
O6 ... H1A	2.008	O7 ... H21B	2.602
O7 ... H3A	1.955	C22 ... H11B	2.547
O7 ... H11C	2.593	C1 ... H32B	2.713
O9 ... H11C	2.509	C10 ... H39B	2.762
O9 ... H3A	2.483	C21 ... H39B	2.710
C11 ... C11	3.350	N14 ... H14B	2.490
H4 ... H4	2.074	C1 ... C7	3.332
		C6 ... C6	3.399

For complex 2, there are also many short interactions that were detected as red spots in the d_{norm} map. In this compound, there are two molecules used as an asymmetric formula; hence, there are two results for the Hirshfeld analysis in this case (Figure 11). Similar to complex 1, the H ... H, O ... H and H ... C contacts are the most dominant. Their percentages are in the ranges of 56.1–56.6, 22.0–22.5 and 8.6–8.8%, respectively. There are many other contacts that are depicted in Figure 8, but their percentages were relatively small. Among the whole of the interactions which occurred in the crystal of complex 2, the O ... H, N ... H, H ... C and C ... C contacts were considered short and appeared as red regions in the d_{norm} map (Figure 11). The fingerprint plots shown in Figure 12 amply indicate the importance of these contacts. O2 ... H3 (1.802 Å), N14 ... H14B (2.490 Å), C22 ... H11B (2.547 Å) and C1 ... C7 (3.332 Å) are the shortest of these interactions (Table 4).

**Figure 11.** Hirshfeld maps of complex 2. The most important interactions are (A) O ... H, (B) N ... H, (C) C ... C and (D) H ... C.

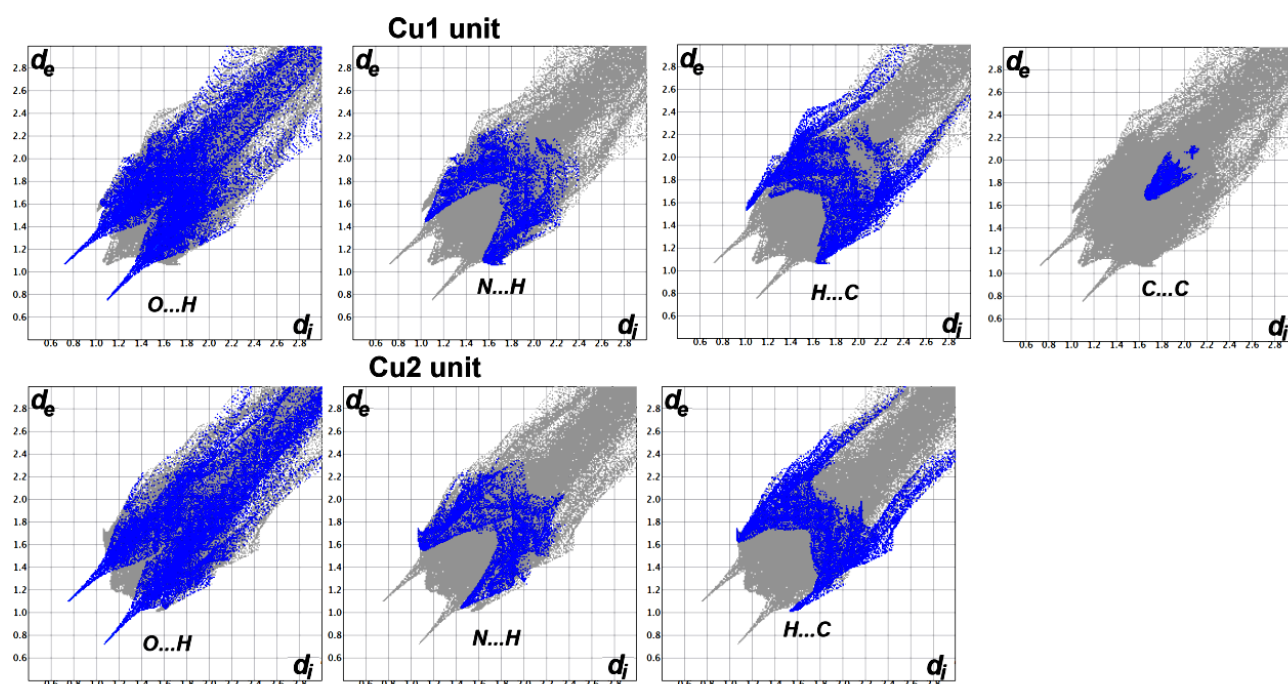


Figure 12. Decomposed fingerprint plots in complex 2.

2.4. XPS Study

XPS analysis is a potent, surface-sensitive method used for checking the chemical composition and purity of atoms, and it can be used to determine the core electron binding energy of atoms within a surface layer up to 10 nm. The correlation between the binding energy (BE) and the atomic potential provides information concerning atoms' oxidation states [56–58]. The wide-ranging scan XPS spectra of the free ligands (**DMAT**, **DMOHT**) and their copper (II) complexes are displayed in Figure S5 (Supplementary material) and the individual contributions within the high-resolution spectra for the different XPS parameters that were collected at 1253.6 eV for Cu(2p_{3/2}), Cu(2p_{1/2}), C1s, O1s and N1s are given in Tables S2 and S3 (Supplementary material). The XPS spectrum for the free ligand (**DMAT**) displays three peaks resulting from the binding energies (BEs) of C1s, N1s and O1s at 286.17, 399.75 and 532.94 eV, respectively. The high-resolution C1s spectra are characterized by contributions at 287.05, 284.71 and 289.37 eV in **DMAT** arising from the C–H, C = C (sp² bonded carbons), C–C (sp³ bonded carbons) and C–N moieties. The de-convolution of the N1s peak shows two peaks, one at 399.45 and another at 398.01 eV, which can be attributed to triazine C = N and NH confirming the structure of the ligand. The full scan spectrum of complex 1 exhibits four peaks corresponding to the BEs of C1s, N1s, O1s and Cu2p at 287.22, 400.85, 533.74 and 935.42 eV, respectively (Figure S5; Supplementary material). Cu2p displayed a satellite structure with two characteristic peaks—Cu2p_{3/2} and Cu2p_{1/2} at 934.28 and 954.23 eV, respectively, with a binding energy difference $\Delta(\text{BE}) = 19.95$ eV characteristic in accordance with the data reported for the existence of the Cu(II) oxidation state [59].

The XPS spectrum for the free ligand (**DMOHT**) displays three peaks resulting from the binding energies (BEs) of C1s (286.24 eV), N1s (399.94 eV) and O1s (533.13 eV) because of C–C (sp³), C–H, and C=C (sp²), as well as H–N, C=N and O–C, respectively. The spectra of complex 2 exhibited four peaks corresponding to the BEs of C1s (286.07 eV), N1s (399.87 eV), O1s (532.82 eV) and Cu2p (934.44 eV). The respective values for complex 3 are 285.91, 407.85, 533.16 and 935.44 eV. Cu2p displayed a satellite structure with two characteristic peaks, Cu2p_{3/2} (932.25 eV) and Cu2p_{1/2} (952.14 eV), for complex 2. The respective values for complex 3 are 934.72 and 954.71 eV. As a result, the binding energy difference (ΔBE) is

19.89 eV for complex 2 and 19.99 eV for complex 3. This finding is in agreement with the data reported for the Cu(II) oxidation state [59].

2.5. FTIR Spectra

The FTIR spectra of the free ligands and their Cu(II) complexes are presented in Figures S3 and S4 (Supplementary material). For complex 1, a new band was observed at 3444 cm^{-1} corresponding to the overlapping $\nu(\text{OH})$ modes for the coordinated water and crystal ethanol molecules, while the $\nu(\text{N-H})$ mode of the hydrazone appeared at the same frequency of 3277 cm^{-1} in DMAT and 1. The $\nu(\text{N-H})$ modes of the amino group appeared at the lower frequencies of 3167 and 3112 cm^{-1} in the complex compared to 3434 and 3390 cm^{-1} in the free ligand, respectively. In addition, the FTIR spectrum of complex 1 showed a sharp spectral band at 1620 cm^{-1} which can probably be assigned to the $\nu(\text{C}=\text{N})$ modes while appearing in the free ligand in the spectral range of 1577–1611 cm^{-1} , indicating the coordination of the Cu(II) ion via the triazine and the azomethine nitrogen atoms. The infrared vibrational band appeared at 1386 cm^{-1} in complex 1, which does not appear in the free ligand and could be attributed to the $\nu(\text{N-O})$ stretches of the nitrate group [60].

The FTIR spectra of the free DMOHT ligand demonstrated the $\nu(\text{OH})$ and $\nu(\text{NH})$ modes at 3440 and 3314 cm^{-1} , respectively, while the $\nu(\text{C}=\text{N})$ modes were detected at 1579–1611 cm^{-1} . The $\nu(\text{C}=\text{N})$ modes were slightly shifted to 1614–1570 and 1608–1568 cm^{-1} , respectively. In complex 3, the $\nu(\text{N-O})$ stretches of the nitrate group appeared at 1384 cm^{-1} . On the other hand, two characteristic bands at 1569 and 1362 resulted from the asymmetric $\nu(\text{COO})$ and symmetric $\nu(\text{COO})$ stretching frequencies in complex 2. The difference [$\Delta\nu = \nu(\text{COO})_{\text{asym}} - \nu(\text{COO})_{\text{sym}} = 207 \text{ cm}^{-1}$] indicates a monodentate coordination mode in the acetato group.

2.6. Biological Studies

2.6.1. Antimicrobial Activity

The antimicrobial activity of the free ligands and the corresponding Cu(II) complexes was determined against different categories of microbes (Table 5). All inhibition zones were determined at 10 mg/mL of the tested compounds. The results indicated that both ligands were not active at the concentration of 10 mg/mL, while the corresponding Cu(II) complexes showed different antimicrobial actions against the tested microbes. Complex 2 showed broad antimicrobial activity against all tested microbes. The largest inhibition zones were found for *B. subtilis* (25 mm), which is very close to the standard Gentamycin (26 mm). The same complex also showed good antifungal activity against *A. fumigatus* (15 mm) while the corresponding value for the standard Ketoconazole used as a control is 17 mm. Complex 1 evidenced antimicrobial activity against all microbes except *C. albicans*. The best result for this complex was found to be against *B. subtilis* (25 mm). On the other hand, complex 3 showed no antifungal activity against either *A. fumigatus* or *C. albicans*, while its antibacterial action remained evident. Likewise, the best result for this complex was found to be against *B. subtilis* (24 mm).

Table 5. Inhibition zone diameters (mm) for the tested microbes ^a.

Microbe	Type	DMAT	DMOHT	1	2	3	Control
<i>A. fumigatus</i>	Fungi	NA *	NA *	14	15	NA	17 ^a
<i>C. albicans</i>		NA *	NA *	NA	10	NA	20 ^a
<i>S. aureus</i>	Gram positive bacteria	NA *	NA *	10	11	12	24 ^b
<i>B. subtilis</i>		NA *	NA *	25	25	24	26 ^b
<i>E. coli</i>	Gram negative bacteria	NA *	NA *	11	14	15	30 ^b
<i>P. vulgaris</i>		NA *	NA *	15	15	13	25 ^b

^a Ketoconazole and ^b Gentamycin, * NA: Not active.

The antimicrobial activity levels of complexes 1–3 were further revealed by determining the Minimum Inhibitory Concentrations (MIC) in $\mu\text{g}/\text{mL}$. The results indicate the strongest actions for all three complexes were against *B. subtilis*. The MIC values in these cases were found to be 39.06, 39.06 and 78.125 $\mu\text{g}/\text{mL}$, respectively, while for Gentamycin the MIC value is 4.8 $\mu\text{g}/\text{mL}$. Regarding the level of antifungal activity, complex 2 exhibited the best results against *A. fumigatus* (625 $\mu\text{g}/\text{mL}$) while the control Ketoconazole has MIC of 156.25 $\mu\text{g}/\text{mL}$ (Table 6).

Table 6. MIC values ($\mu\text{g}/\text{mL}$) for the studied compounds.

Microbe	1	2	3	Control
<i>A. fumigatus</i>	1250	625	ND *	156.25 ^a
<i>C. albicans</i>	ND*	5000	ND *	312.5 ^a
<i>S. aureus</i>	2500	1250	1250	9.7 ^b
<i>B. subtilis</i>	39.06	39.06	78.125	4.8 ^b
<i>E. coli</i>	2500	1250	312.5	4.8 ^b
<i>P. vulgaris</i>	625	1250	1250	4.8 ^b

* ND: Not determined ^a Ketoconazole ^b Gentamycin.

2.6.2. Antioxidant Activity

The studied Cu(II) complexes and the free ligands were assessed for their antioxidant activity levels using an α,α -diphenyl- β -picrylhydrazyl (DPPH) scavenging assay, and the results are given in Table 7. All compounds possessed some antioxidant activity. The results indicated better antioxidant activity for **DMAT** than for **DMOHT**, indicating the effect of the substituent at the phenyl moiety on the antioxidant activity level of the free ligand. The IC_{50} values were determined to be $17.83 \pm 0.65 \mu\text{g}/\text{mL}$ and $48.2 \pm 1.086 \mu\text{g}/\text{mL}$, respectively. On the other hand, the Cu(II) complexes have improved levels of antioxidant activity compared to the free ligands. Complex 1 has an IC_{50} value of $13.34 \pm 0.58 \mu\text{g}/\text{mL}$, which is lower than that of the free **DMAT**. Additionally, complexes 2 and 3 have lower IC_{50} values of 20.93 ± 0.91 and $19.31 \pm 0.73 \mu\text{g}/\text{mL}$, respectively, compared to **DMOHT**. Hence, the Cu(II) complexes appear to be better candidates for antioxidant agents than the free ligands, and 1 is the best performing among the studied Cu(II) complexes when compared with the standard ascorbic acid ($\text{IC}_{50} = 10.62 \pm 0.84 \mu\text{g}/\text{mL}$).

Table 7. The antioxidant activity of the studied compounds.

Conc. ($\mu\text{g}/\text{mL}$)	Ascorbic Acid	DPPH Scavenging %				
		DMAT	DMOHT	1	2	3
1280	98.91	95.31	93.87	96.84	94.54	95.76
640	97.83	94.08	88.54	95.07	92.15	94.29
320	95.64	91.37	84.93	92.48	88.03	90.81
160	92.31	86.59	73.64	87.65	83.14	85.92
80	90.25	79.28	61.32	82.31	78.62	81.47
40	83.09	70.89	47.09	77.49	67.84	68.9
20	71.38	54.23	31.95	68.61	49.08	51.32
10	48.52	35.17	19.87	40.93	36.52	32.95
5	40.36	28.65	10.48	27.86	17.66	18.73
2.5	34.57	20.79	5.73	21.32	9.39	11.46
IC_{50}	10.62 ± 0.84	17.83 ± 0.65	48.2 ± 1.08	13.34 ± 0.58	20.93 ± 0.91	19.31 ± 0.73

2.6.3. Anticancer Activity

The studied compounds were examined for their anticancer activity against the lung carcinoma A-549 cell line. Detailed results are depicted in Tables S4–S8 and summarized graphically in Figure 13. The free ligands **DMAT** and **DMOHT** have large IC_{50} values of $551.48 \pm 27.20 \mu\text{M}$ and $564.51 \pm 30.94 \mu\text{M}$, respectively, indicating a slightly better level of anticancer activity for **DMAT** than for **DMOHT**. In contrast, all the Cu(II) complexes showed good levels of anticancer activity as indicated by their lower IC_{50} values when com-

pared to the free ligands. The IC_{50} value was the best for complex **1** ($5.94 \pm 0.58 \mu\text{M}$) while the corresponding values for complexes **2** and **3** were $141.47 \pm 3.24 \mu\text{M}$ and $58.34 \pm 3.87 \mu\text{M}$, respectively. Hence, the order of the anticancer activity for studied compounds is **1** > **3** > **2** > **DMAT** > **DMOHT**. For *cis*-platin, the IC_{50} value is $25.01 \pm 2.29 \mu\text{M}$, indicating that complex **1** had four times higher anticancer activity than the standard *cis*-platin.

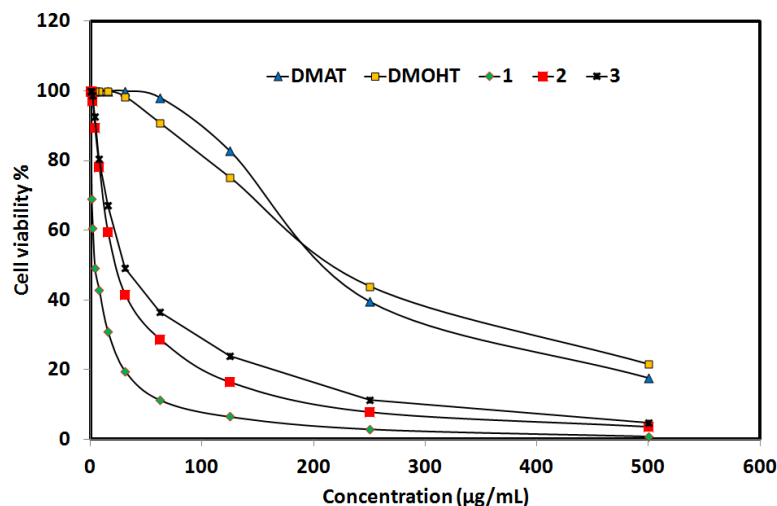


Figure 13. The anticancer activity of the studied compounds versus *Lung carcinoma*.

Additionally, the degree of inhibitory cytotoxic activity against normal human lung fibroblast MRC-5 cells was determined and the results were collected in Tables S9–S13 and presented graphically in Figure 14. The CC_{50} values for indicating the degree of cytotoxic activity are $716.04 \pm 49.36 \mu\text{M}$ and $999.90 \pm 57.13 \mu\text{M}$ for the free **DMAT** and **DMOHT**, respectively. For complexes **1–3**, the CC_{50} values are $37.67 \pm 2.97 \mu\text{M}$, $101.47 \pm 7.01 \mu\text{M}$ and $172.96 \pm 11.98 \mu\text{M}$, respectively. Based on these results, complex **1** shows the highest degree of cytotoxicity against the MRC-5 cell line. In this regard, the selectivity index (SI) was calculated as the ratio of cytotoxic effect on the normal cell line to the cytotoxic effect on the cancer cell line. The SI results revealed that complex **1** had the highest value (6.34) when compared with complexes **2** (0.72) and **3** (2.97). The SI values for the free ligands **DMAT** and **DMOHT** are 1.30 and 1.77, respectively. Hence, complex **1** is the best candidate for consideration as an anticancer agent against lung carcinoma (Table 8).

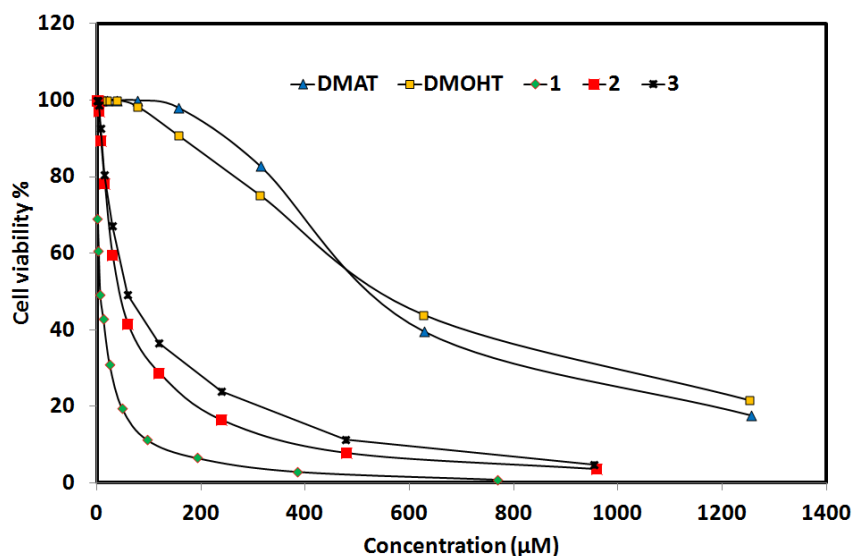


Figure 14. The cytotoxic activity of the studied compounds against normal human lung fibroblast MRC-5 cells.

Table 8. IC₅₀, CC₅₀ and selectivity index (SI) values (μM) for the studied compounds.

	DMAT	DMOHT	Complex 1	Complex 2	Complex 3	<i>cis</i> -Platin
IC ₅₀	551.48	564.51	5.94	141.47	58.34	25.01
CC ₅₀	716.04	999.90	37.67	101.47	172.96	242.25
SI = CC ₅₀ /IC ₅₀	1.30	1.77	6.34	0.72	2.96	9.69

3. Materials and Methods

Fourier transform infrared (FTIR) spectra were recorded on a Nicolet 6700 spectrophotometer in the spectral range of 400–4000 cm⁻¹ at a spectral resolution of 2 cm⁻¹ and with 40 scans per sample. The powder samples were measured in KBr pellets. Further details regarding materials and methods are presented in the Supplementary material.

3.1. Synthesis of Ligands

The two ligands **DMAT** and **DMOHT** were prepared following our previously reported method described in Method S1 (Supplementary material) [55].

3.2. Syntheses of Cu(II) Complexes

All complexes were prepared using the self-assembly of the functional ligand shown in Figure 1 with the corresponding Cu(II) salt.

3.2.1. Synthesis of Complex 1

An ethanolic solution (10 mL) of **DMAT** (79.7 mg, 0.2 mmol) was added to 48.32 mg of Cu(NO₃)₂·3H₂O in (5 mL) ethanol. The clear deep blue solution was left for slow evaporation at room temperature. After ten days, complex 1 was formed as dark blue crystals. **C₂₁H₃₄CuN₁₀O₁₀** (**1**; 650.12 g/mol): Yield; 83%. Anal. Calc. C, 38.80; H, 5.27; N, 21.55; Cu, 9.77%. Found: C, 38.58; H, 5.19; N, 21.41; Cu, 9.65%. IR (KBr, cm⁻¹): 3444, 3277, 3167, 3112, 1620, 1550 and 1386.

3.2.2. Synthesis of Complex 2

A methanolic solution (10 mL) of **DMOHT** (79.9 mg, 0.2 mmol) was added to 24.5 mg of Cu(CH₃COO)₂ in (5 mL) methanol. The clear deep blue solution was left for slow evaporation at room temperature. After five days, complex 2 formed as dark blue crystals. **C₂₁H₂₇CuN₇O₅** (**2**; 521.03 g/mol): Yield; 79%. Anal. Calc. C, 48.41; H, 5.22; N, 18.82; Cu, 12.20%. Found: C, 48.17; H, 5.14; N, 18.68; Cu, 12.09%. IR (KBr, cm⁻¹): 3437, 1614, 1570, 1508 and 1441.

3.2.3. Synthesis of [Cu(DMOT)(NO₃)] Complex 3

Synthesis of this complex was performed the same way as described in **1**. In this case, several trials to obtain good quality crystals suitable for single-crystal structure measurements failed. **C₁₉H₂₄CuN₈O₆** (**3**; 523.99 g/mol): Yield; 87%. Anal. Calc. C, 43.55; H, 4.62; N, 21.38; Cu, 12.13%. Found: C, 43.21; H, 4.53; N, 21.15; Cu, 12.02%. IR (KBr, cm⁻¹): 3436, 1608, 1568 and 1384.

3.3. Hirshfeld Surface Analysis

Hirshfeld surface analyses were performed using Crystal Explorer 17.5 software [61].

3.4. Biological Studies

The antimicrobial, antioxidant and anticancer activities of the studied compounds are described in Methods S2–S4 (Supplementary material).

4. Conclusions

The biological evaluations of the antimicrobial, antioxidant and anticancer activities for two *s*-Triazine Schiff base ligands and their Cu(II) complexes were examined. The structures

of the newly synthesized complexes were determined using different analytical and spectroscopic techniques to be $[\text{Cu}(\text{DMAT})(\text{H}_2\text{O})(\text{NO}_3)]\text{NO}_3 \cdot \text{C}_2\text{H}_5\text{OH}$, $[\text{Cu}(\text{DMOT})(\text{CH}_3\text{COO})]$ (**2**) and $[\text{Cu}(\text{DMOT})(\text{NO}_3)]$ (**3**). The molecular and supramolecular structures of **1** and **2** were described on the basis of X-ray single-crystal diffraction and Hirshfeld analysis. While complex **1** had a hexa-coordinated CuN_3O_3 coordination environment, complex **2** had a CuN_2O_2 tetra-coordinated $\text{Cu}(\text{II})$ ion. Complex **1** ($\text{IC}_{50} = 5.94 \pm 0.58 \mu\text{M}$) had a four times higher level of anticancer activity against lung carcinoma A-549 than did *cis*-platin ($\text{IC}_{50} = 25.01 \pm 2.29 \mu\text{M}$). In addition, the selectivity index of **1** (6.34) was the highest, indicating that complex **1** is the best candidate for use as an anticancer agent against the lung carcinoma A-549 cell line. The same complex also had the highest amount of antioxidant activity compared to ascorbic acid as a control. Both the organic ligands had no antimicrobial activity at the applied concentration. In contrast, the $\text{Cu}(\text{II})$ complexes showed interesting antimicrobial activity against the studied microbes. The three complexes all evidenced a strong antibacterial activity towards *B. subtilis*.

Supplementary Materials: The following supporting information can be downloaded at <https://www.mdpi.com/article/10.3390/molecules27092989/s1>, Materials and physical measurements, X-ray photoelectron spectroscopy (XPS) measurement, Single-crystal X-ray diffraction analysis and structure determination, Figure S1: ^1H and ^{13}C NMR spectra of **DMAT**, Figure S2: ^1H and ^{13}C NMR spectra of **DMOHT**, Figure S3: FTIR spectra of the free **DMAT** and complex **1**, Figure S4: FTIR spectra of the free **DMOHT**, complexes **2** and **3**, Figure S5: XPS spectra for **DMAT**, **DMOHT**, Complexes **1**, **2** and **3**, Table S1: Crystal data and refinement details of the studied complexes, Table S2: The percentages of different contacts in the crystal structure of complexes **1** and **2**, Table S3: XPS analysis of **DMAT** and complex **1**, Table S4: XPS analysis of **DMOHT**, complexes **2** and **3**, Table S5: Inhibitory activity against Lung carcinoma A-549 cells for **DMAT**, Table S6: Inhibitory activity against Lung carcinoma A-549 cells for **DMAT**, Table S7: Inhibitory activity against Lung carcinoma A-549 cells for **DMOHT**, Table S8: Inhibitory activity against Lung carcinoma A-549 cells for **2**, Table S9: Inhibitory activity against Lung carcinoma A-549 cells for **DMAT**, Table S10: Inhibitory activity against Lung carcinoma MRC-5 cells for **DMAT**, Table S11: Inhibitory activity against Lung carcinoma MRC-5 cells for **1**, Table S12: Inhibitory activity against Lung carcinoma MRC-5 cells for **DMOHT**, Table S13: Inhibitory activity against Lung carcinoma MRC-5 cells for **2**, Table S14: Inhibitory activity against Lung carcinoma cells for **3**, Method S1: Preparation of the studied ligands, Method S2: Antimicrobial studies, Method S3: DPPH Radical Scavenging Activity, Method S4: Evaluation of Cytotoxic activity.

Author Contributions: The work was designed and supervised by A.E.-D., T.E.K. and S.M.S.; X-ray structure analyses were performed by S.M.S.; syntheses of complexes were carried out by T.E.K., S.M.S. and N.A.K.; A.E.-F. and K.A.D. carried out the preparations of the organic ligands and their analyses. All authors have read and agreed to the published version of the manuscript.

Funding: This research received no external funding.

Institutional Review Board Statement: Not applicable.

Informed Consent Statement: Not applicable.

Data Availability Statement: Not applicable.

Acknowledgments: We would like to acknowledge Frau. Sabine Foro for performing the single-crystal X-ray structure measurements at FB Material Wissenschaft, FG Strukturforschung, Technische Universitaet Darmstadt, Germany.

Conflicts of Interest: The authors declare no conflict of interest.

Sample Availability: Samples of the compounds are not available from the authors.

References

1. Lv, Y.; Meng, J.; Li, C.; Wang, X.; Ye, Y.; Sun, K. Update on the Synthesis of N-Heterocycles via Cyclization of Hydrazones (2017–2021). *Adv. Synth. Catal.* **2021**, *363*, 5235–5265. [[CrossRef](#)]
2. Asif, M. Pharmacologically potentials of hydrazone containing compounds: A promising scaffold. *Int. J. Adv. Chem.* **2014**, *2*, 85–103. [[CrossRef](#)]

3. Tok, F.; Sağlık, B.N.; Özkay, Y.; İlgin, S.; Kaplancıklı, Z.A.; Kaymakçioğlu, B. Synthesis of new hydrazone derivatives and evaluation of their monoamine oxidase inhibitory activity. *Bioorg. Chem.* **2021**, *114*, 105038. [[CrossRef](#)] [[PubMed](#)]
4. Sharma, P.C.; Sharma, D.; Sharma, A.; Saini, N.; Goyal, R.; Ola, M.; Chawla, R.; Thakur, V.K. Hydrazone comprising compounds as promising anti-infective agents: Chemistry and structure-property relationship. *Mater. Today Chem.* **2020**, *18*, 100349. [[CrossRef](#)]
5. Lawrence, M.A.; Lorraine, S.C.; Wilson, K.A.; Wilson, K. Voltammetric properties and applications of hydrazones and azo moieties. *Polyhedron* **2019**, *173*, 114111. [[CrossRef](#)]
6. Mali, S.N.; Thorat, B.R.; Gupta, D.R.; Pandey, A. Mini-Review of the Importance of Hydrazides and Their Derivatives-Synthesis and Biological Activity. *Eng. Proc.* **2021**, *11*, 21.
7. Zhai, P.; Li, W.; Lin, J.; Li, X.; Wei, W.L.; Chen, W. Hydrazones as Substrates in the Synthesis of Isoxazolidines via a KOH-Promoted One-Pot Three-Component Cycloaddition with Nitroso Compounds and Olefins. *J. Org. Chem.* **2021**, *86*, 17710–17721. [[CrossRef](#)]
8. Suvarapu, L.N.; Seo, Y.K.; Baek, S.O.; Ammireddy, V.R. Review on analytical and biological applications of hydrazones and their metal complexes. *E-J. Chem.* **2012**, *9*, 1288–1304. [[CrossRef](#)]
9. Cao, W.; Liu, Y.; Zhang, T.; Jia, J. Synthesis, characterization, theoretical and antimicrobial studies of tridentate hydrazone metal complexes of Zn (II), Cd (II), Cu (II) and Co (III). *Polyhedron* **2018**, *147*, 62–68. [[CrossRef](#)]
10. Bedia, K.K.; Elçin, O.; Seda, U.; Fatma, K.; Nathaly, S.; Sevim, R.; Dimoglo, A. Synthesis and characterization of novel hydrazide-hydrazones and the study of their structure-antituberculosis activity. *Eur. J. Med. Chem.* **2006**, *41*, 1253–1261. [[CrossRef](#)]
11. Hussain, I.; Ullah, A.; Khan, A.U.; Khan, W.U.; Ullah, R. Synthesis, characterization and biological activities of hydrazone schiff base and its novel metals complexes. *Sains Malays.* **2019**, *48*, 1439–1446. [[CrossRef](#)]
12. Iskander, M.F.; Khalil, T.E.; Foro, S. Synthesis, characterization and X-ray crystal structures of nickel (II) and copper (II) complexes derived from salicylaldehyde cyanoacetylhydrazone. An unexpected ligand transformation. *Inorg. Chim. Acta* **2016**, *453*, 633–646. [[CrossRef](#)]
13. Wu, S.; Zhang, Y.F.; Ding, H.; Li, X.; Lang, X. Hydrazone-linked 2D porphyrinic covalent organic framework photocatalysis for visible light-driven aerobic oxidation of amines to imines. *J. Colloid Interface Sci.* **2022**, *610*, 44654. [[CrossRef](#)] [[PubMed](#)]
14. Khattab, T.A. From chromic switchable hydrazones to smart materials. *Mater. Chem. Phys.* **2020**, *254*, 123456. [[CrossRef](#)]
15. Singh, R.B.; Jain, P.; Singh, R.P. Hydrazones as analytical reagents: A review. *Talanta* **1982**, *29*, 77–84. [[CrossRef](#)]
16. Wahbeh, J.; Milkowski, S. The use of hydrazones for biomedical applications. *Slas Technol. Transl. Life Sci. Innov.* **2019**, *24*, 161–168. [[CrossRef](#)]
17. Rollas, S.; Küçükgülzel, S.G. Biological activities of hydrazone derivatives. *Molecules* **2007**, *12*, 1910–1939. [[CrossRef](#)]
18. Ali, M.R.; Marella, A.; Alam, M.T.; Naz, R.; Akhter, M.; Shaquiquzzaman, M.; Saha, R.; Tanwar, O.; Alam, M.M.; Hooda, J. Review of biological activities of hydrazones. *Indones. J. Pharm.* **2012**, *23*, 193–202.
19. Oliveira, C.B.J.; França, T.C.; LaPlante, S.R.; Villar, J.D. Synthesis and biological activity of hydrazones and derivatives: A review. *Mini. Rev. Med. Chem.* **2020**, *20*, 342–368.
20. Gemma, S.; Kukreja, G.; Fattorusso, C.; Persico, M.; Romano, M.P.; Altarelli, M.; Savini, L.; Campiani, G.; Fattorusso, E.; Basilico, N.; et al. Synthesis of N1-arylidene-N2-quinolyl-and N2-acrydinyldiazones as potent antimalarial agents active against CQ-resistant *P. falciparum* strains. *Bioorg. Med. Chem. Lett.* **2006**, *16*, 5384–5388. [[CrossRef](#)]
21. Lasri, J.; Haukka, M.; Al-Rasheed, H.H.; Abutaha, N.; El-Faham, A.; Soliman, S.M. Synthesis, structure and in vitro anticancer activity of Pd(II) complex of pyrazolyl-s-triazine ligand; A new example of metal-mediated hydrolysis of s-Triazine pincer ligand. *Crystals* **2021**, *11*, 119. [[CrossRef](#)]
22. Yu, M.H.; Liu, X.T.; Space, B.; Chang, Z.; Bu, X.H. Metal-organic materials with triazine-based ligands: From structures to properties and applications. *Coord. Chem. Rev.* **2021**, *427*, 213518. [[CrossRef](#)]
23. Hoog, P.; Gamez, P.; Driessen, W.L.; Reedijk, J. New polydentate and polynucleating N-donor ligands from amines and 2,4,6-trichloro-1,3,5-triazine. *Tetrahedron Lett.* **2002**, *43*, 6783–6786. [[CrossRef](#)]
24. Patel, R.V.; Kumari, P.; Rajani, D.P.; Chikhaliya, K.H. Synthesis, characterization and pharmacological activities of 2-[4-cyano-(3-trifluoromethyl) phenyl amino]-4-(4-quinoline/coumarin-4-yloxy)-6-(fluoropiperaziny)-s-triazines. *J. Fluor. Chem.* **2011**, *132*, 617–627. [[CrossRef](#)]
25. Gamez, P.; Reedijk, J. 1,3,5-Triazine-based synthons in supramolecular chemistry. *Eur. J. Inorg. Chem.* **2006**, *2006*, 29–42. [[CrossRef](#)]
26. Yang, C.; Chen, X.M.; Zhang, W.H.; Chen, J.; Yang, Y.S.; Gong, M.L. Synthesis, crystal structure and luminescence properties of a europium(III) complex with a new planar aromatic tridentate N3 ligand. *J. Chem. Soc. Dalton Trans.* **1996**, *8*, 1767–1768. [[CrossRef](#)]
27. Barakat, A.; El-Faham, A.; Haukka, M.; Al-Majid, A.M.; Soliman, S.M. s-Triazine pincer ligands: Synthesis of their metal complexes, coordination behavior, and applications. *Appl. Organomet. Chem.* **2021**, *35*, e6317. [[CrossRef](#)]
28. Mooibroek, T.J.; Gamez, P. The s-Triazine ring, a remarkable unit to generate supramolecular interactions. *Inorg. Chim. Acta* **2007**, *360*, 381–404. [[CrossRef](#)]
29. Ghosh, C.; Nandi, A.; Basu, S. Supramolecular self-assembly of triazine-based small molecules: Targeting the endoplasmic reticulum in cancer cells. *Nanoscale* **2019**, *11*, 3326–3335. [[CrossRef](#)]
30. Feringán, B.; Termine, R.; Golemme, A.; Granadino, J.M.; Navarro, A.; Giménez, R.; Sierra, T. Triphenylamine-and triazine-containing hydrogen bonded complexes: Liquid crystalline supramolecular semiconductors. *J. Mater. Chem. C* **2021**, *9*, 1972–1982. [[CrossRef](#)]
31. Blotny, G. Recent applications of 2,4,6-trichloro-1,3,5-triazine and its derivatives in organic synthesis. *Tetrahedron* **2006**, *62*, 9507–9522. [[CrossRef](#)]

32. Kolesinska, B.; Kaminski, Z.J. The umpolung of substituent effect in nucleophilic aromatic substitution. A new approach to the synthesis of N, N-disubstituted melamines (triazine triskelions) under mild reaction conditions. *Tetrahedron* **2009**, *65*, 3573–3576. [[CrossRef](#)]
33. Das, A.; Demeshko, S.; Dechert, S.; Meyer, F. A New Triazine-Based Tricompartamental Ligand for Stepwise Assembly of Mononuclear, Dinuclear, and 1D-Polymeric Heptacoordinate Manganese(II)/Azido Complexes. *Eur. J. Inorg. Chem.* **2011**, *2011*, 1240–1248. [[CrossRef](#)]
34. Beilstein, P.; Cook, A.M.; Huetter, R. Determination of seventeen *s*-Triazine herbicides and derivatives by high-pressure liquid chromatography. *J. Agric. Food Chem.* **1981**, *29*, 1132–1135. [[CrossRef](#)]
35. Giacomelli, G.; Porcheddu, A.; Luca, L.D. [1,3,5]-Triazine: A versatile heterocycle in current applications of organic chemistry. *Curr. Org. Chem.* **2004**, *8*, 1497–1519. [[CrossRef](#)]
36. Singh, S.; Mandal, M.K.; Masih, A.; Saha, A.; Ghosh, S.K.; Bhat, H.R.; Singh, U.P. 1,3,5-Triazine: A versatile pharmacophore with diverse biological activities. *Arch. Pharm.* **2021**, *354*, 2000363. [[CrossRef](#)]
37. Solankee, A.; Kapadia, K.; Ćirić, A.; Soković, M.; Doytchinova, I.; Geronikaki, A. Synthesis of some new *s*-Triazine based chalcones and their derivatives as potent antimicrobial agents. *Eur. J. Med. Chem.* **2010**, *45*, 510–518. [[CrossRef](#)]
38. Barakat, A.; El-Senduny, F.F.; Almarhoon, Z.; Al-Rasheed, H.H.; Badria, F.A.; Al-Majid, A.M.; Ghabbour, H.A.; El-Faham, A. Synthesis, X-ray crystal structures, and preliminary antiproliferative activities of new *s*-Triazine-hydroxybenzylidene hydrazone derivatives. *J. Chem.* **2019**, *2019*, 9403908. [[CrossRef](#)]
39. Al-Rasheed, H.; Dahlous, K.; Sharma, A.; Sholkamy, E.; El-Faham, A.; Torre, B.G.; Albericio, F. Barbiturate-and Thiobarbiturate-based *s*-Triazine hydrazone derivatives with promising antiproliferative activities. *ACS Omega* **2020**, *5*, 15805–15811. [[CrossRef](#)]
40. Menear, K.A.; Gomez, S.; Malagu, K.; Bailey, C.; Blackburn, K.; Cockcroft, X.L.; Ewen, S.; Fundo, A.; Gall, A.; Hermann, G.; et al. Identification and optimisation of novel and selective small molecular weight kinase inhibitors of mTOR. *Bioorganic Med. Chem. Lett.* **2009**, *19*, 5898–5901. [[CrossRef](#)]
41. Bai, F.; Liu, H.; Tong, L.; Zhou, W.; Liu, L.; Zhao, Z.; Liu, X.; Jiang, H.; Wang, X.; Xie, H.; et al. Discovery of novel selective inhibitors for EGFR-T790M/L858R. *Bioorganic Med. Chem. Lett.* **2012**, *22*, 1365–1370. [[CrossRef](#)] [[PubMed](#)]
42. Shanmugakala, R.; Tharmaraj, P.; Sheela, C.D.; Anitha, C. Synthesis and studies on *s*-Triazine-based ligand and its metal complexes. *Int. J. Inorg. Chem.* **2012**, *2012*, 301086. [[CrossRef](#)]
43. Samy, F.; Taha, A. Synthesis, Spectroscopic, Biological and Theoretical Studies of Nano Complexes Derived from Triazine Hydrazone. *Egypt. J. Chem.* **2018**, *61*, 731–746.
44. Fouad, R.; Adly, O.M. Novel Cu²⁺ and Zn²⁺ nanocomplexes drug based on hydrazone ligand bearings chromone and triazine moieties: Structural, spectral, DFT, molecular docking and cytotoxic studies. *J. Mol. Struct.* **2021**, *1225*, 129158. [[CrossRef](#)]
45. Samy, F.; Shebl, M. Synthesis, spectroscopic, biological, and theoretical studies of new complexes from (E)-3-(2-(5, 6-diphenyl-1, 2, 4-triazin-3-yl) hydrazono) butan-2-one oxime. *Appl. Organomet. Chem.* **2020**, *34*, e5502. [[CrossRef](#)]
46. Wu, P.; He, Y.; Wang, H.; Zhou, Y.G.; Yu, Z. Copper (II)-Catalyzed C–H Nitrogenation/Annulation Cascade of Ketene N, S-Acetals with Aryldiazonium Salts: A Direct Access to N2-Substituted Triazole and Triazine Derivatives. *Org. Lett.* **2019**, *22*, 310–315. [[CrossRef](#)]
47. Crisponi, G.; Nurchi, V.M.; Fanni, D.; Gerosa, C.; Nemolato, S.; Faa, G. Copper-related diseases: From chemistry to molecular pathology. *Coord. Chem. Rev.* **2010**, *254*, 876–889. [[CrossRef](#)]
48. Iakovidis, I.; Delimaris, I.; Piperakis, S.M. Copper and its complexes in medicine: A biochemical approach. *Mol. Biol. Int.* **2011**, *2011*, 594529. [[CrossRef](#)]
49. Daniel, K.G.; Gupta, P.; Harbach, R.H.; Guida, W.C.; Dou, Q.P. Organic copper complexes as a new class of proteasome inhibitors and apoptosis inducers in human cancer cells. *Biochem. Pharmacol.* **2004**, *67*, 1139–1151. [[CrossRef](#)]
50. Balamurugan, K.; Schaffner, W. Copper homeostasis in eukaryotes: Teetering on a tightrope. *Biochim. Biophys. Acta Mol. Cell Res.* **2006**, *1763*, 737–746. [[CrossRef](#)]
51. Adams, J.Y.; Keen, C.L. Copper, oxidative stress, and human health. *Mol. Asp. Med.* **2005**, *26*, 268–298. [[CrossRef](#)] [[PubMed](#)]
52. Arredondo, M.; Núñez, M.T. Iron and copper metabolism. *Mol. Asp. Med.* **2005**, *26*, 313–327. [[CrossRef](#)] [[PubMed](#)]
53. Noyce, J.O.; Michels, H.; Keevil, C.W. Inactivation of influenza A virus on copper versus stainless steel surfaces. *Appl. Environ. Microbiol.* **2007**, *73*, 2748–2750. [[CrossRef](#)] [[PubMed](#)]
54. Lowndes, S.A.; Harris, A.L. The role of copper in tumour angiogenesis. *J. Mammary Gland Biol. Neoplasia* **2005**, *10*, 299–310. [[CrossRef](#)] [[PubMed](#)]
55. El-Faham, A.; Soliman, S.M.; Ghabbour, H.A.; Elnakady, Y.A.; Mohaya, T.A.; Siddiqui, M.R.H.; Albericio, F. Ultrasonic promoted synthesis of novel *s*-Triazine-Schiff base derivatives; molecular structure, spectroscopic studies, and their preliminary antiproliferative activities. *J. Mol. Str.* **2016**, *1125*, 121–135. [[CrossRef](#)]
56. Heide, P.V. *X-ray Photoelectron Spectroscopy: An Introduction to Principles and Practices*; John Wiley & Sons, Inc.: Hoboken, NJ, USA, 2012; pp. 3–6.
57. Brown, D.G.; Weser, U. XPS Spectra of Copper and Nickel Biuret Complexes—Observations of Intense Satellite Structure in the 2P Spectrum of a Copper(III) System. *J. Inorg. Biochem.* **1979**, *34*, 989–994. [[CrossRef](#)]
58. Biesinger, M.C.; Payne, B.P.; Grosvenor, A.P.; Lau, L.W.M.; Gerson, A.R.; Smart, R.S.C. Resolving surface chemical states in XPS analysis of first row transition metals, oxides and hydroxides: Cr, Mn, Fe, Co and Ni. *Appl. Surf. Sci.* **2011**, *257*, 2717–2730. [[CrossRef](#)]

59. Haber, V.; Ptáček, P. XPS study of metal complexes with an unsymmetrical tetradentate Schiff base. *Inorg. Chim. Acta* **1991**, *179*, 267–270. [[CrossRef](#)]
60. Nakamoto, K. *Infrared and Raman Spectra of Inorganic and Coordination Compounds Part B: Applications in Coordination, Organometallic, and Bioinorganic Chemistry*, 6th ed.; John Wiley & Sons, Inc.: Hoboken, NJ, USA, 2009.
61. Turner, M.J.; McKinnon, J.J.; Wolff, S.K.; Grimwood, D.J.; Spackman, P.R.; Jayatilaka, D.; Spackman, M.A. *Crystal Explorer17*; University of Western Australia: Perth, Australia, 2017; Available online: <https://crystalexplorer.scb.uwa.edu.au/> (accessed on 20 July 2020).